Field Tests for Evaluating the Inherent High-Order Harmonic Resonance of Traction Power Supply Systems up to 5000 Hz

QIUJIANG LIU [ID], (Member, IEEE), **JING LI** [ID], (Student Member, IEEE), **AND MINGLI WU** [ID], (Member, IEEE)

School of Electrical Engineering, Beijing Jiaotong University, Beijing 100044, China

Corresponding author: Mingli Wu (mlwu@bjtu.edu.cn)

ABSTRACT The inherent resonant frequency of a traction power supply system (TPSS) needs to be accurately identified in order to provide crucial information for resonance suppression, safe operation, and system optimization of electrified railways. In this paper, implementation of experiments was carried out in actual railway systems to evaluate the inherent harmonic resonances of the TPSS. The field tests were based on a harmonic generator (HG) constructed with cascaded H-bridge converters (CHBCs). Compared to other experimental setups, the field tests of this paper, which were performed in the 25kV practical system, can provide straightforward results in a wide frequency range up to 5000 Hz. Such a wide frequency range is necessary for assessing and taking effective measures to address the harmonic resonance problem. The results of this paper will supply valuable data for the modeling of TPSSs and the stability analysis of train converters contributing to improvement of the power quality of electric railways.

INDEX TERMS Electric railway, field test, frequency scanning, harmonic resonance, high-order harmonic.

I. INTRODUCTION

It has been reported that the high-order harmonic resonant accidents of electrical railways occurred in many countries, such as New Zealand [1], Korea [2], Britain [3], Italy [4], [5], Spain [6], Thailand [7], China [8]–[10] and so on. This kind of accidents has become serious threat to the safe and stable operation of railways [11], [12]. Therefore, it is of great significance to take effective measures to suppress these resonant accidents and improve the power quality of railways.

The existing research on the resonance between the power supply lines and trains mainly involves two aspects. The first is to analyze the inherent high-order harmonic resonance characteristic of the traction power supply system (TPSS). The second will be discussed in next paragraph. The first part is about the modeling method [13]–[15] of the power supply lines based on the short circuit impedance model of power grid, the traction transformer model, the auto-transformer (AT) model, and multi-conductor transmission lines theory. Then via widely used software such as MATLAB

The associate editor coordinating the review of this manuscript and approving it for publication was Dinesh Kumar [ID].

[16], PSCAD [17], [18], EMTDC [5], [19] or programming by researchers themselves [20], the harmonic resonance of railways is evaluated. However, these modeling methods and the precision of their calculation results are difficult to be verified since few effective filed tests are available. Specifically, on the one hand, the railway is a single phase high voltage system at 25 kV. Thus, some experimental results under low voltage (e.g. 200 V in [21] and 400 V in [19]) cannot represent its characteristics very well. On the other hand, the frequency range of interest is wide and it should at least cover 750Hz-3750Hz [11]; in the experiments based on nonlinear loads switching, e.g. transformers [22], capacitors [23], [24], thyristors [25], the interference will sharply decrease to 0.02 p.u. above 500 Hz which means the experiments are only effective at relatively low frequencies. The success of a harmonic simulation depends critically on the data used to model each power system component. Therefore measurement techniques have being considered to have a great influence on the harmonic resonance evaluation [25]. In this paper, experiments about the inherent high-order harmonic resonance characteristic of the TPSS were carried out based on a harmonic generator (HG), which can generate

TABLE 1. Comparison of experimental setups in actual systems.

Literature	Test method or device	Frequency range	Voltage Level	Actual railway
This paper	Full controlled HG	< 5000Hz	25kV	Yes
[19]	Uninterrupted Power Supply (UPS)	<1250Hz	400V	Yes
[21]	Short circuit experiments	Not mentioned	200V	Yes
[22]	Transformer switching	< 1500Hz	25kV	No
[23]	Capacitor switching	< 950Hz	63.5kV	No
[25]	6 pulse rectifier	$50 \times (6k \pm 1)$, $0 \leq k \leq 6$	10kV	No

FIGURE 1. TPSS schematic diagram of the simplest single-track railway and its distributed model.

the harmonic disturbances with full controlled magnitudes and frequencies. As shown in Tab. 1, compared to other literatures, experimental setups of this paper were performed in the actual 25 kV railway system up to 5000 Hz. In such a wide frequency range, the implementation of field tests will provide effective validation for modeling of traction power supply systems.

As mentioned above, in the research fields of high-order harmonic resonance of railways, the second aspect lies in increasing stability of train converters by improving control strategies and optimizing the main circuits (e.g. increasing the sampling frequency [26], decreasing the control time delay [27], or installing LCL filters [28]). A widely used criterion for stability of grid connected converters is that the real component of the VSC input admittance $Y(j\omega)$ is positive in all frequencies, seen from the point of common coupling. The inherent harmonic resonance of the TPSS plays a significant role in $Y(j\omega)$ [29]–[31]. In other words, the resonant frequency and its corresponding impedance magnitude influence the stability of converters strongly. However, in existing literatures, the inherent harmonic resonance of the TPSS is usually represented by an inductance with a parallel capacitance [32]. This simple circuit can introduce only one parallel resonance whose resonant frequency is commonly set below Nyquist frequency of the converter control system. Unfortunately, the simple circuit has a great gap with practical situations in railway systems. As we presented in Fig.8, the actual TPSS can exhibit more than one parallel resonance and the resonant frequencies are generally higher than Nyquist frequency of train converters. Consequently, many existing studies are not suitable for resonant cases in railway systems. Some researchers from ABB have recognized and tried to explore this problem [29]. In order to promote stability analysis of railway converters, it is necessary to consider a more accurate TPSS resonant model based on field test data. Hence, this paper provides basic and reliable data about the harmonic resonance of TPSSs up to 5000 Hz which is much higher than the Nyquist frequency of train converters.

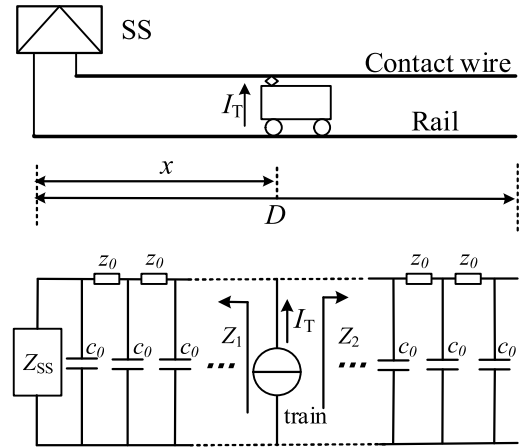The remainder of this paper is organized as follows. In Section II, qualitative analysis based on the simplified

distributed model is presented. In Section III, the test implementations are described including working principles of the test method, the topology of the HG, structures and parameters of the railway under test. Section IV presents and analyzes the test results in detail to provide valuable information. Finally, some conclusions are drawn in Section V.

II. RESONANCE DESCRIPTION BASED ON THE SIMPLIFIED DISTRIBUTED MODEL

In order to explain the principle of high-order harmonic resonance briefly and intuitively, a diagram of the single-track railway, which is the simplest TPSS, is given in Fig. 1 where the SS supplies single phase 25 kV power to the train.

The traction network can be represented as the distributed model, where Z_{SS} represents the equivalent inner impedance of the SS (including the power system and the TT impedance), z_0 and c_0 represent the series impedance and parallel capacitance per unit length of the traction network, respectively, x is the distance between the train and the SS, D is the total length of the traction network, Z_1 and Z_2 are the equivalent input impedances of the TPSS on the left and right sides of the train, respectively, and I_T is the current absorbed by the train. Then, based on Fig. 1 and formulas of wave impedance, the input impedance Z_1 and Z_2 can be calculated as:

$$\begin{cases} Z_1 = Z_c \dfrac{Z_{SS}\cosh(\gamma x) + Z_c\sinh(\gamma x)}{Z_{SS}\sinh(\gamma x) + Z_c\cosh(\gamma x)} \\ Z_2 = \dfrac{Z_c}{\tanh(D - x)}. \end{cases} \tag{1}$$

In (1), Z_c and γ are the characteristic impedance and the transmission coefficient respectively which are derived as:

$$\begin{cases} Z_c = \sqrt{\dfrac{z_0}{j\omega c_0}} = \sqrt{\dfrac{j\omega L_0}{j\omega c_0}} = \sqrt{\dfrac{L_0}{c_0}} \\ \gamma = \sqrt{j\omega c_0 z_0} = j\omega\sqrt{c_0 L_0} \end{cases} \tag{2}$$

where ω is the angular frequency, L_0 is the series inductance per unit length of the traction network (resistor component is

neglected in the simplified model, so $Z_0 = j\omega L_0$). The total input impedance of the TPSS seen from the train is described as:

$$
\begin{aligned}
Z_{\text{in}} &= \frac{Z_1 Z_2}{Z_1 + Z_2} \\
&= Z_c \cosh[\gamma(D - x)]\frac{Z_{\text{SS}}\cosh(\gamma x) + Z_c\sinh(\gamma x)}{Z_{\text{SS}}\sinh(\gamma D) + Z_c\cosh(\gamma D)}.
\end{aligned} \quad (3)
$$

If $|Z_{\text{in}}| \to \infty$, meaning that the input impedance of the TPSS trends to infinity, high-order harmonic parallel resonance will occur. The equipment of a train may be destroyed by the overvoltage caused by this parallel resonance. On the contrary if $|Z_{\text{in}}| \to 0$ it means that serious resonance occurs. This serious resonance barely has a bad influence on the TPSS, so the parallel resonance draws much more attention. In other words, the resonant frequencies can be restated:

$$
\exists \omega \in (0, \omega_c) \text{ makes } Z_{SS}\sinh(\gamma D) + Z_c\cosh(\gamma D) = 0. \quad (4)
$$

In (4), $(0, \omega_c)$ is the frequency range where Z_{SS} is inductive and can be represented by

$$
Z_{\text{SS}} = j\omega L_{\text{SS}}. \quad (5)
$$

Thus, (4) can be deduced as follows:

$$
j\omega L_{\text{SS}} = \frac{-Z_c}{\tanh(\gamma D)}. \quad (6)
$$

By inserting (2) into (6), it is obtained that

$$
-1 = j\omega\sqrt{c_0\frac{L_{\text{SS}}^2}{L_0}}\tanh(j\omega\sqrt{c_0 L_0 D^2}). \quad (7)
$$

By simplifying the hyperbolic tangent function, the following equation is derived as

$$
\frac{\frac{1}{\sqrt{L_{\text{SS}}Dc_0\frac{L_{\text{SS}}}{DL_0}}}}{\omega} = \tan(\sqrt{Dc_0 DL_0}\omega). \quad (8)
$$

Assuming $\frac{L_{\text{SS}}}{DL_0} = k$ and $D\sqrt{c_0 L_0} = \sqrt{Dc_0 DL_0} = \sqrt{C_D L_D}$ where C_D and L_D are total distributed capacitance and inductance of the traction network respectively, k is the proportionality coefficient that L_{SS} is relative to L_D, solutions of equation (8) can be determined by the crossover points of $F(\omega)$ and $G(\omega)$:

$$
\begin{cases}
F(\omega) = \dfrac{\frac{1}{k\sqrt{C_D L_D}}}{\omega} \\
G(\omega) = \tan(\sqrt{C_D L_D}\omega)
\end{cases} \quad 0 < \omega < \omega_c. \quad (9)
$$

From (9), it can be found that $F(\omega)$ is an inverse proportional function and $G(\omega)$ is a tangent function. These two functions are influenced by L_D, C_D and k. Different L_D, C_D and k will result in the stretching transformation of $F(\omega)$ and $G(\omega)$. This indicates that the resonant frequencies are affected by length of the traction network D, distributed parameters per unit length of the traction network L_0 and c_0, the inner impedance of the SS L_{SS}. Considering k increasing from 0.001 to 10, plots of $F(\omega)$ will decrease as shown
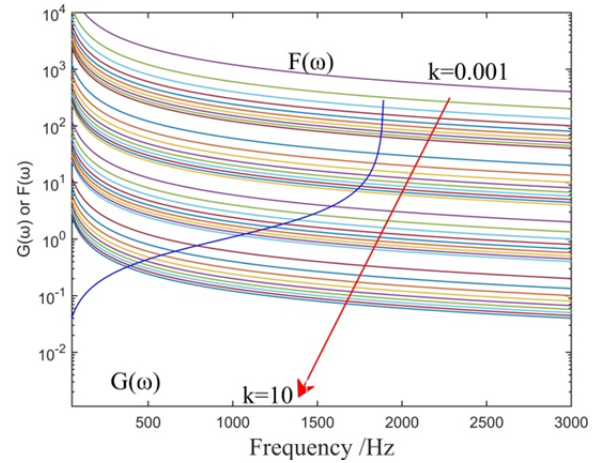

FIGURE 2. Influence of k on the resonant frequency.

in Fig. 2 where D is 25km, c_0 is $0.01796\mu\text{F/km}$, and L_0 is 1.5514mH/km. Then the frequency of the crossover point will also decrease with a nonlinear trend meaning that the resonant frequency is brought down.

The influence analysis of L_D and C_D are similar with that about k which is not presented due to the limited space of this paper. At the specific frequencies, if the following approximation is satisfied

$$
\sqrt{C_D L_D}\omega \sim 0 \quad (10)
$$

then $G(\omega)$ can be deduced as:

$$
\tan(\sqrt{C_D L_D}\omega) \sim \sqrt{C_D L_D}\omega. \quad (11)
$$

As a result, (8) can be simplified as follows:

$$
1 \approx \omega^2 c_0 D L_{\text{SS}}. \quad (12)
$$

The resonant frequency is expressed as:

$$
\omega \approx \frac{1}{\sqrt{c_0 D L_{\text{SS}}}}. \quad (13)
$$

It should be noted that only in the low frequency range, generally speaking <1000Hz, (10) to (12) can be obtained. Based on (9) and (12), the resonance mechanism can be analyzed qualitatively. However, this model is only applicative for the simplest TPSS, as shown in Fig. 1. As for actual TPSSs, such as AT-fed 2 × 25 kV system, an equation like (4) cannot be deduced by hand due to the complexity of traction networks. Therefore, the MTL-based model is developed to study the resonant properties of TPSSs which is capable of dealing with actual railways. However, these methods require the knowledge of comprehensive and correct data concerning network elements and loads in a wide frequency range, since the accuracy of any calculation cannot be better than the data on which it is based. Thus the measurement campaign is necessary. It will be possible to deduce some improvement of the network models, allowing for the missing data and making the computer calculations more reliable.
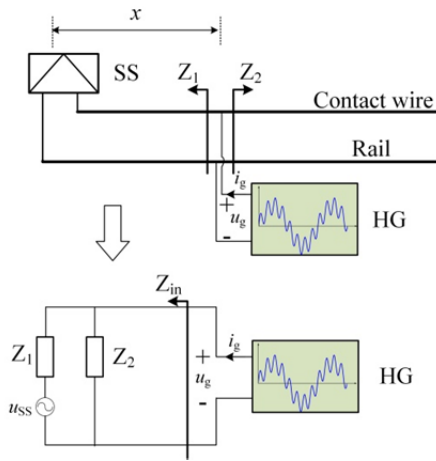
FIGURE 3. Implementation diagram of the test method.

III. IMPLEMENTATION OF FIELD TESTS

A. WORKING PRINCIPLES OF THE TEST METHOD

The test method is based on the frequency-scanning strategy as illustrated in Fig. 3. Locating x km away from SS, the HG, which is represented by the green block, is connected between the contact wire and the rail to inject actively harmonic currents of various frequencies and amplitudes into the TPSS. The frequency of the injected currents is increased step by step with Δf until it covers all the frequencies to be studied. During the test, the generated harmonic current i_g and harmonic voltage u_g are recorded. The FFT algorithm is applied to calculate the amplitudes (U_g, I_g) and phases (θ_u, θ_i) of u_g and i_g at the injected frequency. Then the two amplitudes divide and θ_u subtracts θ_i to obtain the input impedance of the h-order harmonic. After the frequency-scanning test is completed, harmonic impedance Z_{in} can be obtained which represents the parallel impedance of Z_1 and Z_2, as shown in Fig. 3.

A detailed flow chart of the test method is presented in Fig.4. In order to decrease the influence of background harmonics and improve the measurement accuracy, interharmonic is also be selected to inject into TPSS, namely Δf is not the integral multiple of the fundamental frequency. In this paper Δf is set 25 Hz, in other words, the frequencies of actual injected harmonics are 75 Hz, 100 Hz, 125 Hz, 150 Hz, ... In addition, as shown in Fig. 4, the harmonic impedance is averaged over the multiple test data within the 30-second interval for reducing test error.

B. TOPOLOGY AND CONTROL OF THE HG

The HG is the key of the test method as shown in Fig 5. The structure is based on a single-phase H-bridge cascade converter (CHBC) consisting of N cells. Each capacitor voltage, the current and voltage at the ac side are sampled synchronously. The total dc-capacitor voltage of all the cells is maintained to N times of the reference value V_{ref} with the total voltage controller (TVC). The outputs of TVC and the
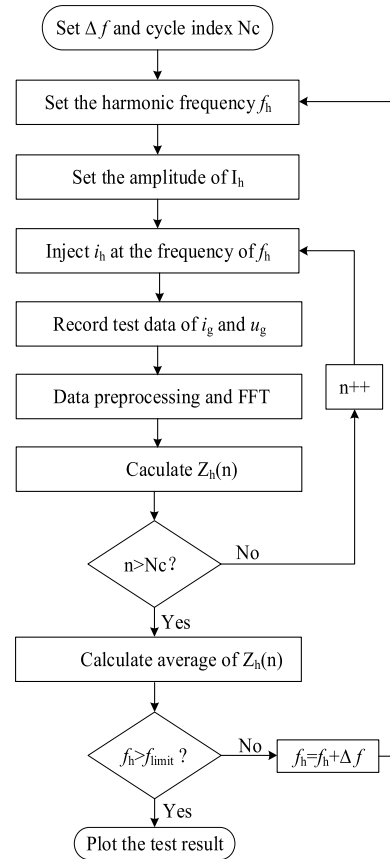

FIGURE 4. Flow chart of the test method.

PLL form the reference value of the current control loop to regulate the output ac current i_g. The current controller (CC) can adopt the proportional resonant controller with a resonant frequency at 50 Hz. A voltage balancing controller (VBC) is used to keep each capacitor voltage to the desired value V_{ref} by shifting active power among these converter cells. The PI controllers are suitable for both TVC and VBC. The ac voltage u_g smoothed by a low pass filter is added to the outputs of VBC and CC. The output sum of VBC, CC and u_g form the primary modulating wave at the fundamental frequency. The harmonic injection controller (HIC) is designed to generate the harmonic modulating wave according to instructions of the desirable harmonic disturbance (f_{href} and I_{href}). Then the total modulating wave including the fundamental and harmonic components is compared with N carrier waves based on Carrier Phase-Shifted PWM (CPS-PWM) drive IGBTs of the HG. The influence of CPS-PWM on the harmonic generating performance has been studied in our previous work [33].

The actual HG in the field that was constructed based on the topology and control methods mentioned above is shown in Fig. 5(b). All the devices including CHBCs, the control system, the inductance, voltage and current sensors are integrated into one container for outdoor operation. The HG is designed as 200 kVA and can inject harmonics in the
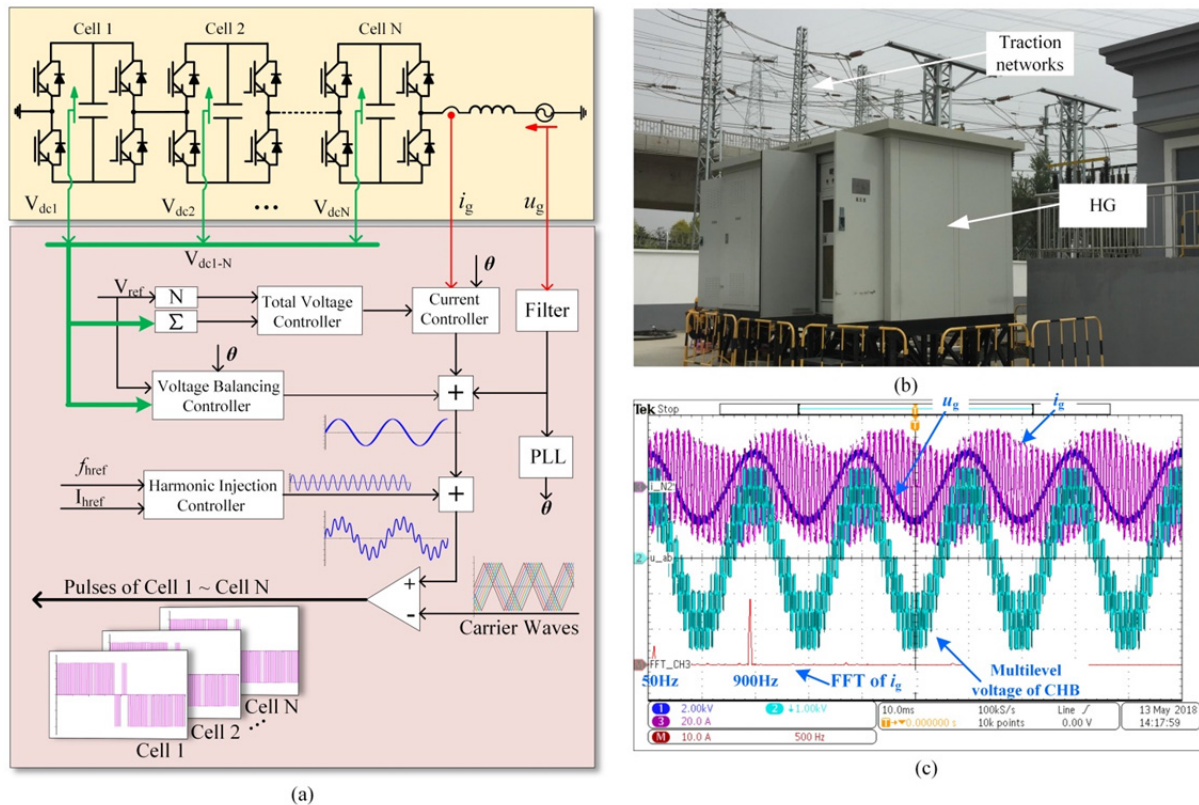
FIGURE 5. CHB-based HG (a) topology and its control strategy, (b) photo of the HG in the field, and (c) waveforms of the HG.

frequency range of <5000 Hz. Taking emitting 900 Hz harmonic current for example; waveforms of the HG are shown in Fig. 5(c) when field tests were being carried out. It clearly can be found that the i_g contains both fundamental and harmonic components. The FFT result of i_g also indicates that the harmonic component at 900 Hz is about three times larger than the fundamental component. Meanwhile, other harmonics can be ignored. This means that a very pure harmonic current was injected into TPSS successfully.

C. THE RAILWAY UNDER TEST
The configuration of the railway under test is shown in Fig. 6 where the voltage of positive feeders (PFs) is -25kV and the voltage of the overhead contact lines (OCLs) is 25kV in normal operation. Autotransformers (ATs) are installed in the middle and at the end of the railway to constitute a 2 × 25 kV AT-feeding system. The total length of the railway is 26.25 km (D=26.25km). The 16 switches S_1-S_{16} are used to cut-off the fault and change the power supply modes. If all the switches were set to be open, the traction network will be disconnected from the substation (SS). In the following tests presented in Section IV, the switches were set to be off or on according the test requirements. The HG was connected between the OCL and the ground of the downgoing direction railway at the SS meaning $x = 0$ in Fig. 3. The photo of the railway under test is shown in Fig.6 (b). The

parameters of the TPSS are listed in Tab.2, where H represents the high voltage winding; L is the low voltage winding of the AT; T and F are the first and the second low voltage windings of the traction transformer respectively.

IV. TEST RESULTS AND ANALYSIS
A. THREE TESTS
Three tests are designed to investigate the mechanism of the inherent resonance of TPSSs (Besides the three in this paper, a series of tests were carried out at the same time for different study purposes which are outside of the scope of this paper. We will discuss the test results in other papers.) As shown in Tab.3, the switching states of S_1-S_{16} were changed to realize the desirable operation modes. More specifically, in the first test, all the switches were set as open. As a result, the HG was connected to SS directly without traction networks as shown in Fig. 7(a). The result Z_1 of Test I reflects the inner harmonic impedance of the SS. In the second test, S_4 was set as closed while others were set as open. Then, the simplified configuration of the railway is shown in Fig. 7(b). In Test II, the railway operation mode was set as the simplest direct supply system with single traction network which is the same as that in Fig. 1. In Test III, only four switches S_1-S_4 were closed. Compared to Test II, double traction networks were to be estimated.
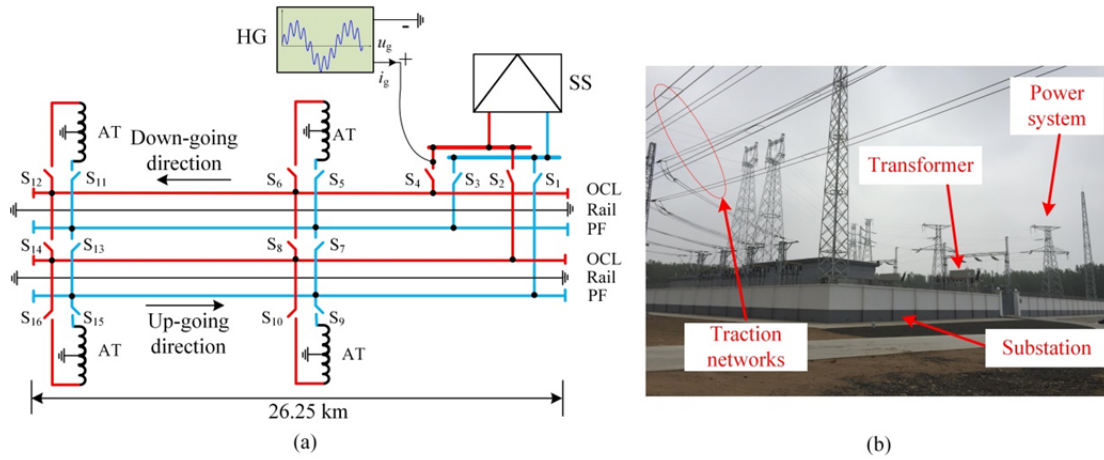
FIGURE 6. The railway under test (a) schematic diagram and (b) photo of the actual railway.

TABLE 2. Parameters of the TPSS.

Component	Item	Parameter
Network wires	OCL	CTMH150
	PF	LGJ400/65
	Rail	P60
AT	Rated power	25/25 MVA (H/L)
	Rated voltage	55/27.5 kV (H/L)
	Rated current	454.5/ 909.0 A (H/L)
	No-load loss	9.552 kW
	No-load current	0.066%
	Load loss	42.114 kW
	Short-circuit Imp.	1.343
Traction transformer	Connection type	I i0 i0
	Rated power	40/40/20 MVA (H/T/F)
	Rated voltage	220/27.5/27.5 kV (H/T/F)
	Rated current	1455/ 727.3 A (T/F)
	No-load loss	22.395 kW
	No-load current	0.06%
	Load loss	88.156 kW
	Short-circuit Imp.	10.59 H-(T+F)
		13.52 H-T
		9.44 H-F

TABLE 3. Switch state of the three tests.

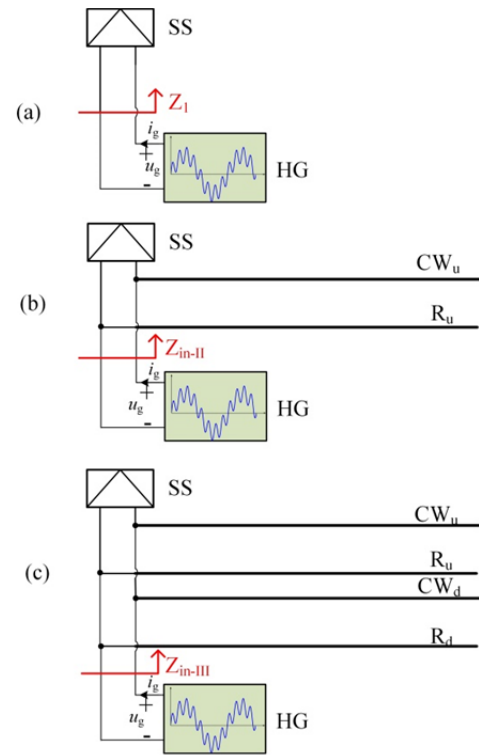| Test	Closed switches	Open switches
I	None	S_1-S_{16}
II	S_4	S_1-S_3, S_5-S_{16}
III	S_2, S_4	S_1, S_3, S_5-S_{16}

FIGURE 7. Schematic diagram of the three tests (a) Tset I, (b) Test II, and (c) Test III.

where $Z_{2-\mathrm{II}}$ and $Z_{2-\mathrm{III}}$ represent the input harmonic impedance of traction networks in Test II and Test III respectively. According to (14), impedance-frequency characteristics of traction networks separated from the SS can be obtained.

B. TEST RESULTS

The test results are presented in Fig.8. It can be found in Fig.8(a) about the first test that below 3000 Hz, the phases

Based on Fig.3 and Fig. 7, relations of Z_1, $Z_{\mathrm{in}-\mathrm{II}}$, and $Z_{\mathrm{in}-\mathrm{III}}$ can be depicted as:

$$Z_{\mathrm{in}\text{-}m} = \frac{Z_1 Z_{2\text{-}m}}{Z_1 + Z_{2\text{-}m}}, \quad m = \mathrm{II}, \mathrm{III} \tag{14}$$
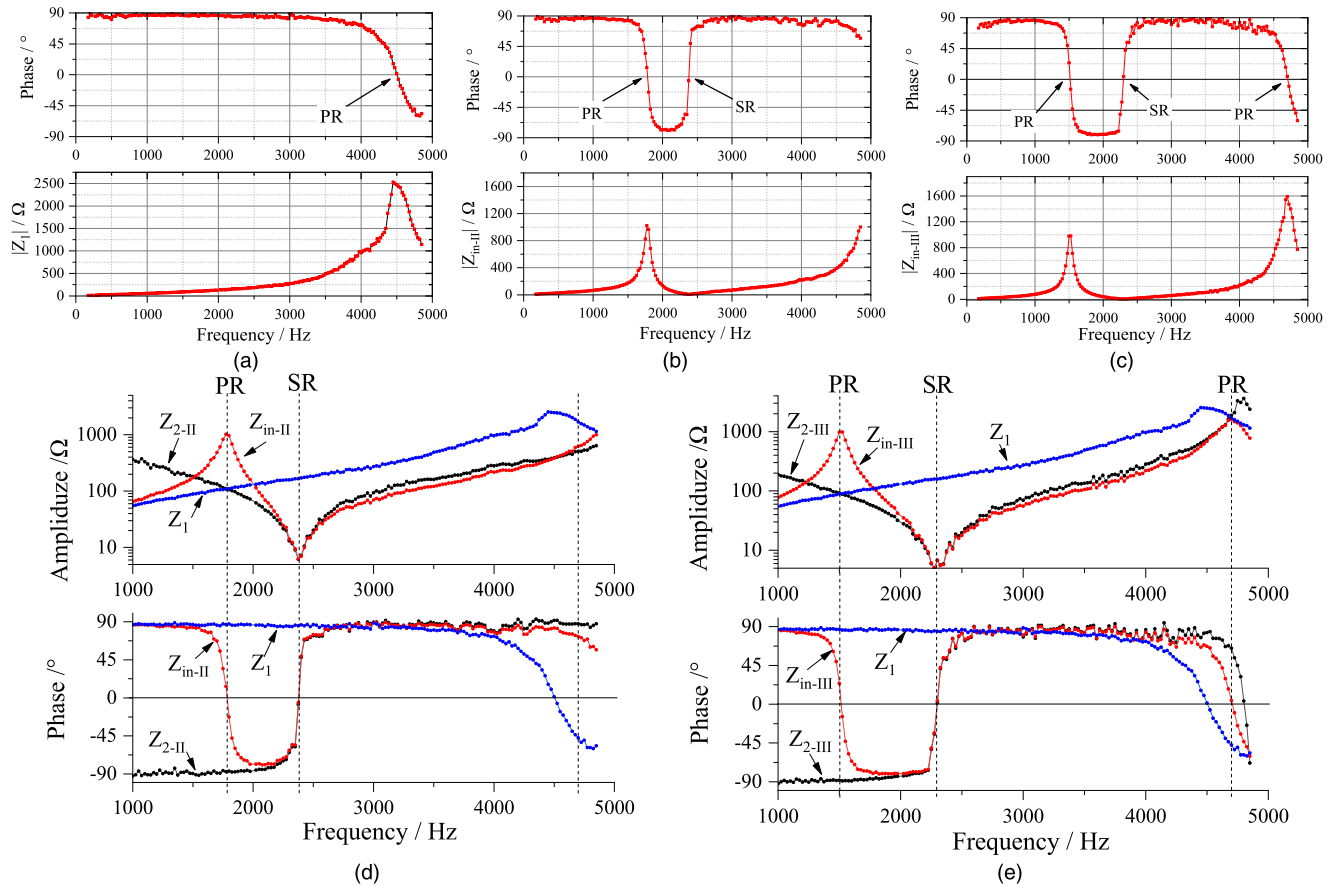
FIGURE 8. Amplitude and phase curves of test results: (a) Test I; (b) Test II; (c) Test III; (d) comparison of Z_1, Z_{2-II}, and Z_{in-II}; (e) comparison of Z_1, Z_{2-III}, and Z_{in-III}.

of Z_1 are very close to 90°, indicating Z_1 can be represented by an inductance. This inductance increases gradually in this frequency range as shown in the second subplot of Fig. 8(a). From 3000Hz to 4450 Hz, Z_1 is still inductive; however, its phase drops to zero and its amplitude increases to the peak sharply at 4450 Hz. Above 4450 Hz, Z_1 becomes capacitive and its amplitude begins to decrease. In other words, Z_1 exhibits an inherent parallel resonance (PR) at 4450 Hz

Fig.8 (b) illustrates the test result Z_{in-II} of Test II. At 1775Hz, the amplitude of Z_{in-II} reaches the maximum value and its phase changes from inductive to capacitive. Thus this property indicates 1775Hz is a PR frequency. At 2375Hz, the phase curve passes through the zero line from negative to positive and the amplitude reaches the minimum value which shows that 2375 Hz is a series resonance (SR) frequency.

Fig.8 (c) describes the test result Z_{in-III} of Test III. The variation trend of Z_{in-III} is very similar to Z_{in-II}. However, compared to Fig. 8(b), there are two PRs in Fig. 8(c). The frequency of the first PR is 1500 Hz which is lower than the first one of Test II.

Based on Figs. 8(a)-(c), we can obtain the straightforward understanding that different structures would influence the resonant frequencies. In order to explain how this works, Figs. 8(d) and (e) can give more information where Z_{2-II} and

Z_{3-II} are deduced based on (14). In Fig.8(d), at the PR point, the amplitudes of Z_1 and Z_{2-II} are equal while their phases are opposite which is as follows:

$$Im(Z_1) + Im(Z_{2\text{-}II}) = 0. \qquad (15)$$

This means that the harmonic power oscillation occurs at 1775Hz between the inductive component of Z_1 and the capacitive component of Z_{2-II}. As a result, PR occurs and the total input impedance is resistive whose phase is zero. In Fig. 8(e), the total equivalent capacitance was increased because of the parallel double track railways as shown in Fig. 7, the imaginary part $Im(Z_{2-III})$ is smaller compared to that of Z_{2-II} at the same frequency according to:

$$|Im(Z_{2\text{-}III})| \propto \frac{1}{(Dc_0)^k}, \quad k > 0 \qquad (16)$$

when Z_{2-II} is capacitive. Consequently, the intersection point of Z_1 and Z_{2-III} will shift to bottom left in the amplitude plot of Fig. 8(e). The corresponding frequency, i.e. the parallel frequency, will decrease. In Fig. 8(e), the second PR occurs at the frequency of 4700 Hz. In contrast to the first one, Z_1 is capacitive and Z_{2-III} is inductive.

The SR of Test II can be explained as following based on Fig. 8(d): at 2375 Hz, Z_{2-II} is nearly zero. As a result, though

Z_1 is large inductive impedance, the total input impedance of the TPSS Z_{in-II} can be calculated as

$$Z_{in-II} = \frac{Z_1 Z_{2-II}}{Z_1 + Z_{2-II}} \approx Z_1 \approx 0. \tag{17}$$

This indicates that the SR is primarily affected by the traction networks. Harmonic power is Ingested and expelled at the SR frequency by the distributed inductance interacting with the distributed capacitance. This situation is the same as Fig. 8(e).

V. CONCLUSION

In this paper, experimental setups were carried out in the actual 25 kV railway system to study the inherent high-order harmonic resonance of TPSSs up to the 100th harmonic. The successful implementation and detailed test results proved the effectiveness of the test system which is based on CHBCs and has the frequency scanning function. Compared to other experiments in existing literatures, the field tests of this paper will provide effective validation for the modeling of TPSSs in a wide frequency range up to 5000 Hz. Meanwhile, the test results also indicate that the stability analysis above Nyquist frequency of train converters should be carefully considered since the TPSS may have several resonant frequencies in that frequency range.

REFERENCES

[1] B. Mellitt, J. Allan, Z. Y. Shao, W. B. Johnson, A. Hooper, and M. R. Denley, "Harmonic characteristics of traction loads on New Zealand's newly electrified north island line," in *Proc. 10th Int. Conf. Electric. Distribut.*, May 1989, pp. 392–396.

[2] H. Lee, C. Lee, G. Jang, and S. Kwon, "Harmonic analysis of the Korean high-speed railway using the eight-port representation model," *IEEE Trans. Power Del.*, vol. 21, no. 2, pp. 979–986, Apr. 2006, doi: 10.1109/TPWRD.2006.870985.

[3] R. Kadhim and D. Kelsey, "25 kV harmonic resonance modelling on channel tunnel rail link," in *Proc. IET Seminar EMC Railways*, Birmingham, U.K., 2006, pp. 137–151, doi: 10.1049/ic:20060195.

[4] A. Dolara, M. Gualdoni, and S. Leva, "Impact of high-voltage primary supply lines in the 2 × 25 kV–50 Hz railway system on the equivalent impedance at pantograph terminals," *IEEE Trans. Power Del.*, vol. 27, no. 1, pp. 164–175, Jan. 2012, doi: 10.1109/TPWRD.2011.2167635.

[5] M. Brenna and F. Foiadelli, "Analysis of the filters installed in the interconnection points between different railway supply systems," *IEEE Trans. Smart Grid*, vol. 3, no. 1, pp. 551–558, Mar. 2012, doi: 10.1109/TSG.2011.2162860.

[6] L. Sainz, L. Monjo, S. Riera, and J. Pedra, "Study of the Steinmetz circuit influence on AC traction system resonance," *IEEE Trans. Power Del.*, vol. 27, no. 4, pp. 2295–2303, Oct. 2012, doi: 10.1109/TPWRD.2012.2211084.

[7] B. Lutrakulwattana, M. Konghirun, and A. Sangswang, "Harmonic resonance assessment of 1×25kV, 50 Hz traction power supply system for suvarnabhumi airport rail link," in *Proc. 18th Int. Conf. Electr. Mach. Syst. (ICEMS)*, Pattaya, Thailand, Oct. 2015, pp. 752–755, doi: 10.1109/ICEMS.2015.7385134.

[8] X. Zhang, J. Chen, G. Zhang, R. Qiu, and Z. Liu, "The WRHE-PWM strategy with minimized THD to suppress high-frequency resonance instability in railway traction power supply system," *IEEE Access*, vol. 7, pp. 104478–104488, 2019, doi: 10.1109/ACCESS.2019.2930969.

[9] J. Li, M. Wu, M. Molinas, K. Song, and Q. Liu, "Assessing high-order harmonic resonance in locomotive-network based on the impedance method," *IEEE Access*, vol. 7, pp. 68119–68131, 2019, doi: 10.1109/ACCESS.2019.2918232.

[10] S. Liu, F. Lin, X. Fang, Z. Yang, and Z. Zhang, "Train impedance reshaping method for suppressing harmonic resonance caused by various harmonic sources in trains-network systems with auxiliary converter of electrical locomotive," *IEEE Access*, vol. 7, pp. 179552–179563, 2019, doi: 10.1109/ACCESS.2019.2958880.

[11] K. Song, W. Mingli, S. Yang, Q. Liu, V. G. Agelidis, and G. Konstantinou, "High-order harmonic resonances in traction power supplies: A review based on railway operational data, measurements, and experience," *IEEE Trans. Power Electron.*, vol. 35, no. 3, pp. 2501–2518, Mar. 2020, doi: 10.1109/TPEL.2019.2928636.

[12] Z. He, H. Hu, Y. Zhang, and S. Gao, "Harmonic resonance assessment to traction power-supply system considering train model in China high-speed railway," *IEEE Trans. Power Del.*, vol. 29, no. 4, pp. 1735–1743, Aug. 2014, doi: 10.1109/TPWRD.2013.2284233.

[13] A. Dolara, M. Gualdoni, and S. Leva, "Reduced multiconductor transmission line models for power quality analysis in railway systems," in *Proc. IEEE 15th Int. Conf. Harmon. Qual. Power*, Jun. 2012, pp. 796–802, doi: 10.1109/ICHQP.2012.6381269.

[14] L. Alfieri, F. Mottola, M. Pagano, and D. Proto, "Harmonic analysis of high-speed railway system for different configurations of the traction power line," in *Proc. AEIT Int. Annu. Conf.*, Oct. 2018, pp. 1–6, doi: 10.23919/AEIT.2018.8577278.

[15] F. Chun-Lei, W. Guang-Ning, Z. Xue-Yuan, and W. Yun-Fei, "The measurement and simulation research of electrified railway harmonic," in *Proc. Int. Conf. Condition Monitor. Diagnosis*, 2008, pp. 1–4, doi: 10.1109/CMD.2008.4580398.

[16] J. Wang, L. Xue, Y. Liu, M. Li, L. Pan, S. Li, S. Wang, and Y. Liu, "The interaction research between public grid and traction power supply system," in *Proc. China Int. Conf. Electr. Distrib.*, Dec. 2008, pp. 1–8, doi: 10.1109/CICED.2008.5211744.

[17] H. Wang, Y. Li, H. Liu, L. Wu, and Y. Sun, "Transmission characteristics of harmonics and negative sequence components of electrified railway in power system," in *Proc. Int. Conf. Smart Grid Clean Energy Technol. (ICSGCE)*, Oct. 2016, pp. 301–306, doi: 10.1109/ICSGCE.2016.7876073.

[18] M. Brenna, F. Foiadelli, and D. Zaninelli, "Electromagnetic model of high speed railway lines for power quality studies," *IEEE Trans. Power Syst.*, vol. 25, no. 3, pp. 1301–1308, Aug. 2010, doi: 10.1109/TPWRS.2010.2042979.

[19] W. Mingli, C. Roberts, and S. Hillmansen, "Modelling of AC feeding systems of electric railways based on a uniform multi-conductor chain circuit topology," in *Proc. IET Conf. Railway Traction Syst. (RTS)*, Birmingham, U.K., 2010, pp. 1–5, doi: 10.1049/ic.2010.0018.

[20] R. Cella, G. Giangaspero, A. Mariscotti, A. Montepagano, P. Pozzobon, M. Ruscelli, and M. Vanti, "Measurement of AT electric railway system currents at power-supply frequency and validation of a multiconductor transmission-line model," *IEEE Trans. Power Del.*, vol. 21, no. 3, pp. 1721–1726, Jul. 2006, doi: 10.1109/TPWRD.2006.874109.

[21] C. Xie, S. B. Tennakoon, R. Langella, D. Gallo, A. Testa, and A. Wixon, "Harmonic impedance measurement of 25 kV single phase AC supply systems," in *Proc. 9th ICHOP*, Oct. 2000, pp. 214–219, doi: 10.1109/ICHQP.2000.897027.

[22] W. Xua, X. Liu, and Y. Liu, "Assessment of harmonic resonance potential for shunt capacitor applications," *Electr. Power Syst. Res.*, vol. 57, no. 2, pp. 97–104, Mar. 2001, doi: 10.1016/S0378-7796(01)00092-X.

[23] A. Baloi, L. Kocewiak, C. L. Bak, and A. Pana, "Experimental determination of harmonic conditions amplification in a distribution network by capacitor bank switching," in *Proc. 13th Int. Conf. Optim. Electr. Electron. Equip. (OPTIM)*, May 2012, pp. 194–199, doi: 10.1109/OPTIM.2012.6231894.

[24] S. Li, Y. Xiao, and J. Cheng, "Dual synchronization incremental method for harmonic impedance measurement," in *Proc. IEEE 15th Int. Conf. Harmon. Qual. Power*, Jun. 2012, pp. 433–437, doi: 10.1109/ICHQP.2012.6381308.

[25] J. Ma, X. Wang, F. Blaabjerg, W. Song, S. Wang, and T. Liu, "Multi-sampling method for single-phase grid-connected cascaded H-bridge inverters," *IEEE Trans. Ind. Electron.*, to be published, doi: 10.1109/TIE.2019.2947864.

[26] J. Yang, J. Liu, Y. Shi, N. Zhao, J. Zhang, L. Fu, and T. Q. Zheng, "Carrier-based digital PWM and multirate technique of a cascaded H-Bridge converter for power electronic traction transformers," *IEEE J. Emerg. Sel. Topics Power Electron.*, vol. 7, no. 2, pp. 1207–1223, Jun. 2019, doi: 10.1109/JESTPE.2019.2891735.

[27] W. Song, S. Jiao, Y. W. Li, J. Wang, and J. Huang, "High-frequency harmonic resonance suppression in high-speed railway through single-phase traction converter with LCL filter," *IEEE Trans. Transport. Electrific.*, vol. 2, no. 3, pp. 347–356, Sep. 2016, doi: 10.1109/TTE.2016.2584921.

[28] L. Harnefors, R. Finger, X. Wang, H. Bai, and F. Blaabjerg, "VSC input-admittance modeling and analysis above the Nyquist frequency for passivity-based stability assessment," *IEEE Trans. Ind. Electron.*, vol. 64, no. 8, pp. 6362–6370, Aug. 2017, doi: 10.1109/TIE.2017.2677353.

[29] C. Zhang, M. Molinas, S. Foyen, J. A. Suul, and I. Takanori, "Harmonic domain SISO equivalent impedance modeling and stability analysis of a single-phase grid connected VSC," *IEEE Trans. Power Electron.*, to be published, doi: 10.1109/TPEL.2020.2970390.

[30] J. Lyu, X. Zhang, X. Cai, and M. Molinas, "Harmonic state-space based small-signal impedance modeling of a modular multilevel converter with consideration of internal harmonic dynamics," *IEEE Trans. Power Electron.*, vol. 34, no. 3, pp. 2134–2148, Mar. 2019, doi: 10.1109/TPEL.2018.2842682.

[31] M. A. Awal, H. Yu, L. D. Flora, W. Yu, S. Lukic, and I. Husain, "Observer based admittance shaping for resonance damping in voltage source converters with LCL filter," in *Proc. IEEE Energy Convers. Congr. Exposit. (ECCE)*, Sep. 2019, pp. 4455–4462, doi: 10.1109/ECCE.2019.8913194.

[32] Q. Liu, M. Wu, J. Li, and J. Zhang, "Controllable harmonic generating method for harmonic impedance measurement of traction power supply systems based on phase shifted PWM," *J. Power Electron.*, vol. 18, no. 4, pp. 1140–1153, Jul. 2018, doi: 10.6113/JPE.2018.18.4.1140.

JING LI (Student Member, IEEE) received the B.Sc. degree in electrical engineering from the North China University of Water Resources and Electric Power, Zhengzhou, China, in 2013, and the M.Sc. degree from Beijing Jiaotong University, Beijing, China, in 2016, where she is currently pursuing the Ph.D. degree in electrical engineering. She was a Visiting Student with the Norwegian University of Science and Technology (NTNU), Trondheim, Norway, from October 2018 to 2019.

Her research interests include power quality of electric railways and power electronics in power supply systems.

QIUJIANG LIU (Member, IEEE) was born in Hebei, China. He received the B.Sc., M.Sc., and Ph.D. degrees in electrical engineering from Beijing Jiaotong University (BJTU), Beijing, China, in 2012, 2014, and 2018, respectively. He is currently a Postdoctoral Researcher with BJTU. His research interests include power quality of electric railways, energy storage systems, and other applications of power electronics in traction power supply systems.

MINGLI WU (Member, IEEE) was born in Hebei, China. He received the B.Sc. and M.Sc. degrees in electrical engineering from Southwest Jiaotong University, Chengdu, China, in 1993 and 1996, respectively, and the Ph.D. degree in electrical engineering from Beijing Jiaotong University, Beijing, China, in 2006.

Since 2008, he has been a Professor with the School of Electrical Engineering, Beijing Jiaotong University. His research interests include power supply for electric railways, digital simulation of power systems, and electric power quality.

• • •